ACS OMEGA

Open Access

http://pubs.acs.org/journal/acsodf

Article

Corrosion Behavior of Carbon Steel in Diethylenetriamine Solution for Post-combustion CO_2 Capture

Xinyue Chen, Yongkang Cui, and Shujuan Wang*

Cite This: *ACS Omega* 2024, 9, 13067−13080

Read Online

ACCESS | Metrics & More | Article Recommendations

ABSTRACT: In the realm of postcombustion carbon capture, diethylenetriamine (DETA), recognized for its substantial CO_2 absorption capacity, presents a formidable challenge due to its corrosive impact on equipment. This study delves into the corrosion behavior of 20# carbon steel immersed in DETA solutions under varying conditions, employing weight loss and electrochemical methods. The investigation incorporates scanning electron microscopy/energy-dispersive spectroscopy and X-ray diffraction analyses for characterization. Corrosion experiments were also conducted in monoethanolamine (MEA) solutions for a comparative analysis. Results from the corrosion tests in DETA solutions mirror the temperature-dependent corrosion rate (CR) observed in MEA. However, a distinctive trend emerges as the CO_2 loading of DETA increases from 0.2 mol CO_2/mol amine to 1.2 mol CO_2/mol amine, leading to a continuous decrease in the CR of carbon steel—contrary to MEA solutions. This anomaly is attributed to DETA's robust complexing ability with metal ions and its elevated solubility of Fe^{2+} in solution. Additionally, an examination of the corrosion mechanism in the presence of oxygen was conducted through characterizing the specimen surface and solution precipitates postexperiment. The absence of a protective $FeCO_3$ layer can be attributed to insufficient concentrations of free Fe^{2+} and CO_3^{2-} in the solution, failing to achieve the minimum saturation required for protective film formation. The insights gained from studying the corrosion behavior of carbon steel in DETA solutions lay the groundwork for subsequent developments in corrosion inhibitors.

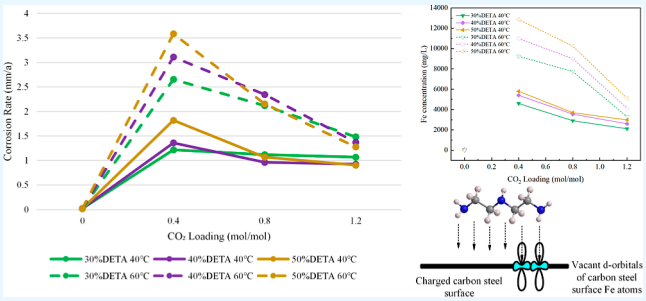

1. INTRODUCTION

The excessive emission of greenhouse gases caused by human activities has caused a serious global warming. CO_2 is the most important greenhouse gas and the main cause of climate change.[1] Addressing this issue, carbon capture and storage (CCS) technology emerges as a promising avenue for curtailing CO_2 and greenhouse gas emissions. Within CCS, postcombustion CO_2 capture, particularly employing chemical absorption with aqueous amine-based solvents, stands as the most established and efficacious method.[2,3]

However, aqueous amine solutions will corrode equipment, which is one of the major issues facing CO_2 capture technology.[4] Corrosion transpires through electrochemical reactions at the metal−electrolyte interface. The anodic reaction involves the metal-losing electrons, whereas the cathodic reaction entails the oxidant-gaining electrons from the metal.[5] While amines exhibit some corrosion inhibition capabilities, they induce severe corrosion of carbon steel equipment under CO_2 capture conditions due to the formation of bicarbonate and carbamate species.[6] Moreover, the presence of 4−8% O_2 in flue gas exacerbates the corrosion extent.[7]

The widely used 30 wt % monoethanolamine (MEA) solvents serve as a benchmark for CO_2 capture, possessing maturity in application. In comparison, diethylenetriamine (DETA) boasts a higher CO_2 absorption capacity and a faster absorption rate due to its three amino groups,[8] essential components in biophysical solvents for CO_2 capture.[9,10] Recognized as potential candidates for energy-efficient CO_2 capture, biphasic solvents, particularly liquid−liquid biphasic absorbents, have been extensively investigated.[11] DETA's relatively high molecular weight and elevated electron density on the nitrogen functional group enable it to act as an electron donor, forming ligand covalent bonds with metal surface electrons,[12] thus rendering it suitable as an organic corrosion inhibitor in weakly alkaline and acidic corrosive media, such as seawater and CO_2-saturated NaCl solutions.[13−15] Consequently, DETA is anticipated to exhibit a high absorption capacity without inducing significant corrosion, promising excellent application prospects.

Received: November 29, 2023
Revised: January 13, 2024
Accepted: February 19, 2024
Published: March 4, 2024

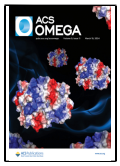

Table 1. Chemical Composition of 20# Carbon Steel

component	C	Si	Mn	S	P	Cr	Ni	Cu	Fe
weight (%)	0.17−0.24	0.17−0.37	0.35−0.65	≤0.035	≤0.035	≤0.25	≤0.25	≤0.20	Bal

While numerous studies have delved into the corrosion behavior of common primary amines (MEA), secondary amines (diethanolamine, DEA), and tertiary amines (methyldiethanolamine, MDEA),[16−18] the corrosion behavior of polyamines such as DETA has received limited attention. Rafat et al.[19] examined the corrosion behaviors of classic amine solutions and new ionic liquids, revealing that the corrosion rate (CR) was determined by the characteristic CO_2 absorption capacity, with MEA > DEA > MDEA under identical conditions. Nainar et al.[20] explored the corrosion of carbon steel in aqueous solutions of MEA and piperazine (PZ), investigating the impact of amine concentration, CO_2 loading, temperature, and the presence of heat-stable salts on the CR. Fischer[21] discussed the influence of Fe^{2+} solubility in different amine solutions on the formation of protective layers on carbon steel surfaces in his doctoral dissertation, emphasizing the difference in Fe^{2+} solubility in MEA and PZ solutions. However, limited research has been conducted on the corrosion of polyamines like DETA. Hayfron-Benjamin E[22] examined the effects of DETA degradation products and temperature on the corrosion behavior of stainless steel, but the variations under different CO_2 loadings were not thoroughly investigated.

Therefore, this study primarily investigates the corrosion behavior and corrosion mechanism of carbon steel in DETA solutions, providing pivotal insights for subsequent research on optimizing working conditions and implementing corrosion inhibition in actual application processes.

2. EXPERIMENTAL SECTION

2.1. Sample and Solution Preparation. Given the inherent corrosion challenges under the operating conditions of the postcombustion CO_2 capture process and the corrosion induced by the absorbent, stainless steel is deemed the optimal material for process equipment.[23] However, considering the substantial cost difference—stainless steel being 3−6 times more expensive than carbon steel—carbon steel remains widely used in practical projects to mitigate the total cost of postcombustion CO_2 capture.[24] This study, focused on unraveling the corrosion behavior of DETA, seeks to establish a foundation for its extensive use in practical engineering. The 20# carbon steel specimen, with its chemical composition (wt %) detailed in Table 1, was chosen as the experimental material. All specimens were sourced from the same batch and obtained from identical pipes.

For both weight loss and electrochemical experiments, type III carbon steel specimens (40 × 13 × 2 mm, surface area 12 cm^2) were utilized. Before the experiments, the specimens underwent polishing, cleaning with ethanol and deionized water, and drying in hot air.

MEA and DETA were provided by Macklin (Shanghai, China) (purity ≥99%). Hydrochloric acid and methenamine, which were used to clean the surface products of the corrosion specimens in the weight loss method, were provided by Tongguang Fine Chemicals (Beijing) and Lanyi Chemicals (Beijing). The 1,10-phenanthroline, hydroxylammonium chloride, acetic acid, and sodium acetate used in the analysis process were obtained from Aladdin (Shanghai, China).

The experiments necessitated aqueous solutions of MEA and DETA, with MEA serving as the comparison group. Varied working conditions encompassed amine concentration, temperature, and CO_2 loading, as detailed in Table 2. Amine concentration adjustments were achieved by altering the mixing ratio of amine to deionized water. Temperature adjustments were made using a water bath, while the CO_2 loading of the amine solution underwent variation through a CO_2 absorption device, as illustrated in Figure 1. To attain the required CO_2 loading, the amine solution was initially saturated with CO_2, and the saturation loading was measured by titration. The titration device, comprising a U-shaped tube and a sealed tank, facilitated a neutralization reaction when excess acid was added. The volume of CO_2 produced equated to the volume of CO_2 absorbed by the measured solution. CO_2 absorption capacity was quantified in units of mol of CO_2/mol of amine. Subsequently, a fresh amine solution was added to achieve the desired CO_2 loading.

Table 2. Different Conditions of the Amine Systems in Experiments

amine	parameter	condition
MEA	temperature (°C)	40, 60
	CO_2 loading (mol CO_2/mol amine)	0.0, 0.4
	amine concentration (%)	30, 40, 50
DETA	temperature (°C)	40, 60
	CO_2 loading (mol CO_2/mol amine)	0.0, 0.4, 0.8, 1.2
	amine concentration (%)	30, 40, 50

2.2. Methods. *2.2.1. Weight Loss Method.* The weight loss method, a well-established technique for assessing equipment corrosion in solution, has seen extensive application in prior studies.[25,26] Preceding the experiment, all 20# carbon steel specimens underwent washing with deionized water and ethanol, subsequent drying, and initial weighing. Various MEA and DETA solutions, featuring distinct amine concentrations and CO_2 loadings, were introduced into 60 mL sample bottles, housing the carbon steel specimens. These sample bottles were immersed in a water bath set at a predetermined temperature for a duration of 30 days. After that, the corroded specimens were extracted, subjected to cleaning procedures conforming to the GB/T16545−2015 standard, and reweighed. It is worth noting that this system cannot eliminate the impact of the presence of oxygen; therefore, the dissolved oxygen has been considered during the analysis and discussion of results. The weight loss method, adept at capturing long-term corrosion behavior in a specific environment, facilitated the computation of the average CR using eq 1

$$CR = \frac{87600 \times (m_0 - m_1)}{A \times \rho \times t} \quad (1)$$

where CR is the corrosion rate (mm/a); m_0 and m_1, respectively, denote the weight of the specimen before and after corrosion (g); A, ρ, and t, respectively, denote the exposed surface area of the specimen (cm^2), sample density (g/cm^3), and corrosion time (h).

https://doi.org/10.1021/acsomega.3c09540
ACS Omega 2024, 9, 13067−13080

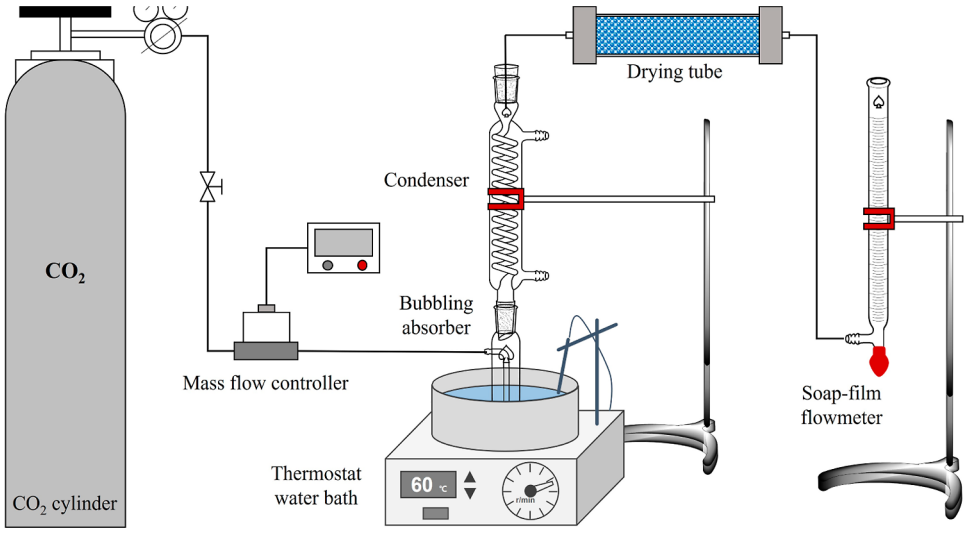

Figure 1. Schematic diagram of the experimental setup for the CO_2 absorption.

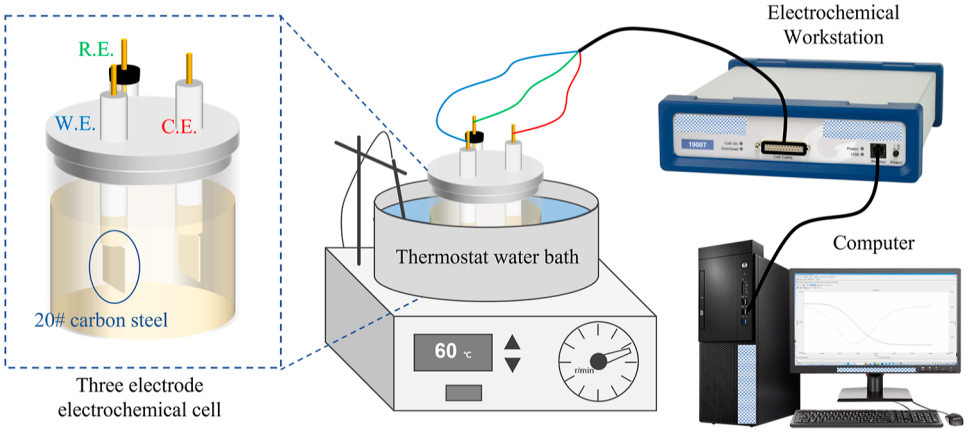

Figure 2. Schematic representation of the experimental setup for the electrochemical corrosion tests.

2.2.2. Electrochemical Testing. While the weight loss method provides actual corrosion rates through extended experiments and characterizes corrosion through various methods, the corrosion process fundamentally involves electrochemical reactions. Electrochemical experiments offer deeper insights into electrochemical corrosion phenomena, delivering a more comprehensive understanding of the reaction process and its influencing factors.[27,28]

A schematic representation of the experimental setup for electrochemical corrosion is presented in Figure 2. Employing a three-electrode electrolytic cell placed within a thermostatic water bath to ensure a constant temperature, the electrochemical corrosion tests were conducted. The working electrode (W.E.) comprised 20# carbon steel in the test solution. The reference electrode utilized was Ag/AgCl (saturated KCl), and a platinum electrode served as the counter electrode. The electrolytic cell, sealed for precision, had its three electrodes electrically connected to an electrochemical workstation (reference 1000, Gamry, USA).

The experimental procedure commenced with the measurement of the open-circuit potential (OCP) until stabilization (~0.1 mV). Electrochemical impedance spectroscopy (EIS) followed at the OCP, employing a perturbation amplitude of 10 mV and scanning across a frequency range of 100 kHz−0.01 Hz. Tafel curve measurements spanned from −250 to +250 mV (versus OCP) with a constant scanning rate of 0.167 mV/s. Tafel curves, anode/cathode polarization curves generated by polarizing the specimen in both anode and cathode directions within a defined potential range, were employed. Electrochemical parameters were derived through Tafel extrapolation to ascertain the corrosion current (i_{corr}). The instantaneous corrosion rate was calculated as CR using eq 2

$$CR = \frac{3.27 \times 10^{-3} \times i_{corr} \times W}{A \times \rho} \quad (2)$$

where CR is the corrosion rate (mm/a); i_{corr} is the corrosion current (μA); W is the equivalent weight (g) of the specimen; and A and ρ represent the W.E. area (cm^2) and specimen density (g/cm^3), respectively. It is noteworthy that the corrosion current serves as the primary determinant of the CR.

2.3. Surface Characterization. In-depth understanding of corrosion and exploration of the corrosion mechanism of 20# carbon steel in DETA solutions necessitated the characterization of corrosion specimens.[29,30] Scanning electron microscopy (SEM) was employed for observing surface morphologies, while energy-dispersive spectrometry (EDS) and X-ray diffraction (XRD) were utilized to analyze the components of corrosion products on specimen surfaces. The surface morphology of carbon steel was characterized by using FE-

https://doi.org/10.1021/acsomega.3c09540
ACS Omega 2024, 9, 13067−13080

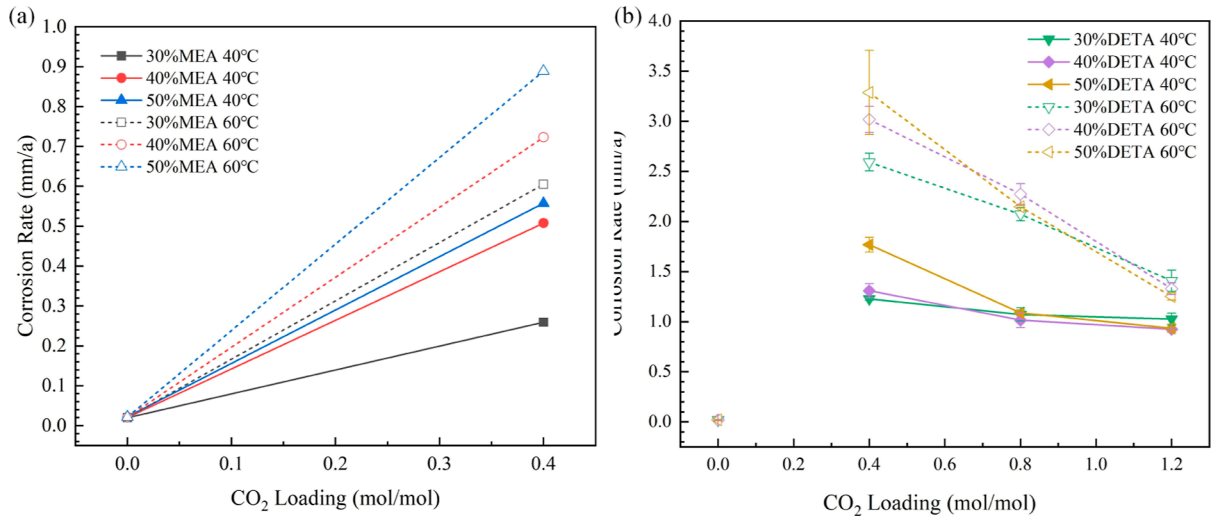

Figure 3. Relationship between the CR of carbon steel and the CO_2 loading of amine solution after corrosion for 30 days calculated by the weight loss method: (a) MEA solution and (b) DETA solution.

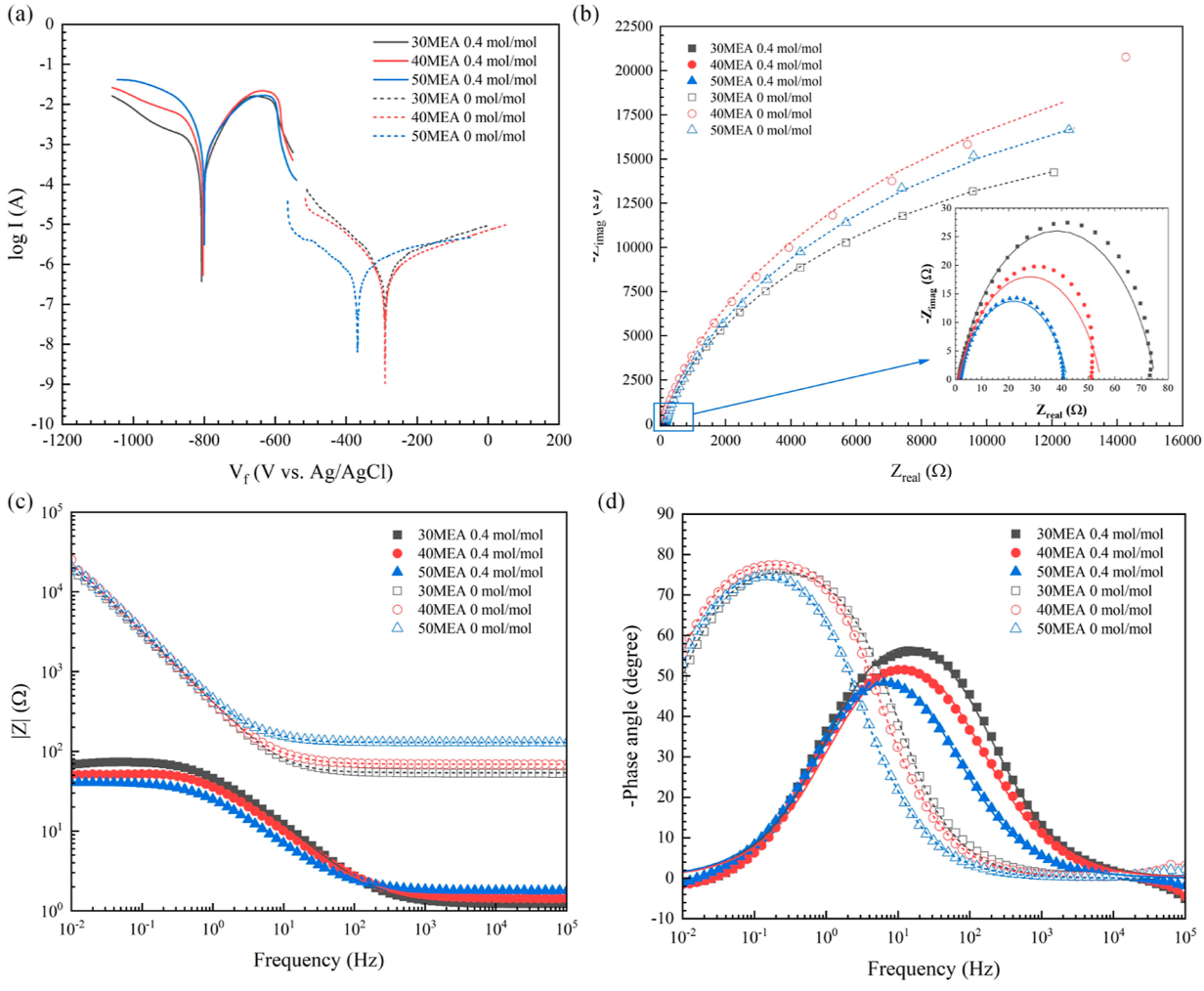

Figure 4. Electrochemical results of 20# carbon steel in MEA solutions under different conditions (60 °C): (a) Tafel curve; (b) Nyquist plots; (c) Bode plots of impedance vs frequency; and (d) Bode plots of phase angle.

SEM (Merlin, Zeiss, Germany). The EDS detector mounted on the SEM instrument facilitated the determination of the elemental composition of the carbon steel surface. XRD (D/max-2550, Rigaku, Japan) operated at a voltage of 40 kV and a current of 40 mA, equipped with a Cu target, with a measurement range spanning from 10° to 90°. Diffraction patterns were analyzed using MDI Jade 6 software with the ICDD PDF-2 version 2012 database.

https://doi.org/10.1021/acsomega.3c09540
ACS Omega 2024, 9, 13067−13080

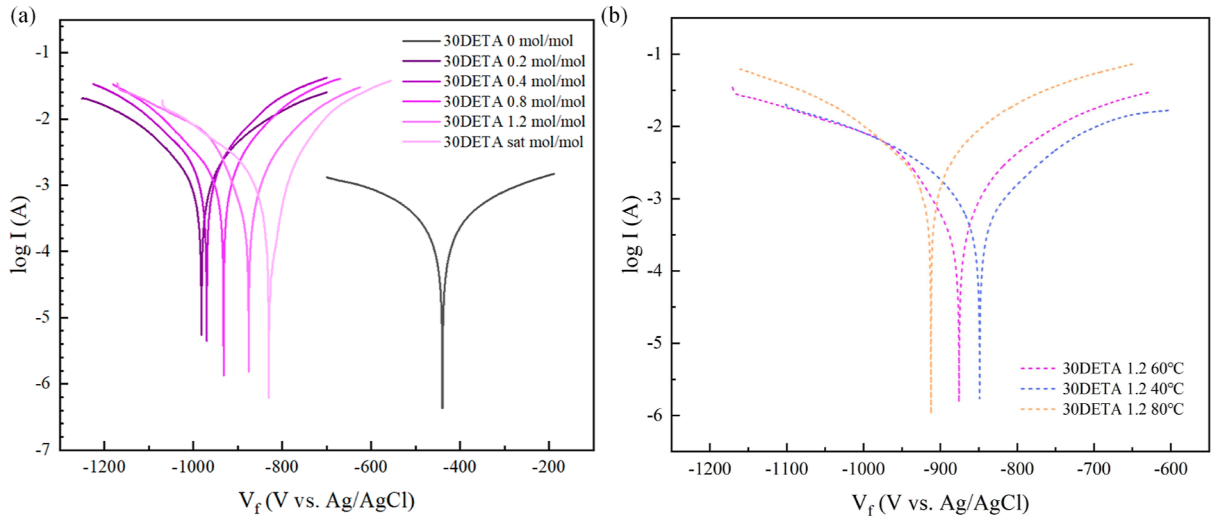

Figure 5. Tafel curves of 20# carbon steel in 30% DETA solutions under different conditions: (a) different CO_2 loadings and (b) different temperatures.

Table 3. Fitted Electrochemical Parameters of Tafel Curves for 20# Carbon Steel in Different Solutions

	condition							
medium	temperature (°C)	CO_2 loading (mol/mol)	E_{OCP} (mV)	E_{corr} (mV)	I_{corr} (mA)	β_a (mV·dec^{-1})	$-\beta_c$ (mV·dec^{-1})	CR (mm/a)
30% MEA	60	0	−270.8	−292.26	1.26×10^{-3}	323.51	141.31	0.00122
		0.4	−801.6	−807.82	0.232	48.27	55.33	0.225
40% MEA		0	−264.5	−286.80	1.12×10^{-3}	358.97	153.58	0.00109
		0.4	−803.3	−803.72	0.463	45.87	62.98	0.448
50% MEA		0	−300.2	−366.76	0.623×10^{-3}	203.72	188.84	0.000604
		0.4	−800.1	−799.99	0.763	43.98	83.22	0.740
30% DETA	40	1.2	−848.9	−842.59	0.852	125.09	146.63	0.825
	60	0	−439.1	−438.62	8.71×10^{-2}	145.92	154.97	0.0845
		0.2	−990.5	−982.70	−2.54	291.04	283.88	2.764
		0.4	−981.3	−972.39	2.73	186.52	211.72	2.644
		0.8	−935.2	−934.90	1.93	152.35	183.29	1.872
		1.2	−881.1	−871.02	1.18	127.06	143.52	1.146
		sat	−812.6	−832.28	0.959	128.924	152.99	0.930
	80	1.2	−912.3	−916.07	2.69	125.11	143.07	2.615

Moreover, SEM and XRD were employed for ex situ characterization of precipitates generated in the solution, such as the blue-black precipitate following 30 days of corrosion in MEA solutions loaded with CO_2. Postexperiment, the precipitate in the solution underwent vacuum filtration and rinsing with deionized water. The extracted solids were dried and characterized in an oven before final analysis.[22]

2.4. Solution Analysis. Utilizing the phenanthroline spectrophotometric method, the concentration of Fe ions in test solution samples was measured using a UV−visible spectrophotometer (Agilent, cary100).[31] The experiments were conducted at least twice, and average values are reported.

3. RESULTS

3.1. Weight Loss Results. The corrosiveness of fresh amine solutions was negligible; however, upon CO_2 absorption, they exhibited corrosion tendencies. This study delved into the corrosion behavior of 20# carbon steel in DETA solutions through weight loss experiments under varying conditions. For comparative reliability, corrosion experiments were conducted on MEA solutions. The long-term corrosion rates, measured using the weight loss method, are depicted in Figure 3. In fresh amine solutions, the corrosion rates of 20# carbon steel were nearly 0 mm/a. Yet, after CO_2 absorption, different phenomena emerged in the MEA and DETA solutions. With escalating temperature, the corrosion rates of specimens under identical conditions gradually increased, attributed to accelerated oxidation and reduction reactions at the anode and cathode with rising temperature.[32] Interestingly, an increase in CO_2 loading resulted in opposing trends in the corrosion rates of 20# carbon steel in MEA and DETA solutions. In MEA solutions, more CO_2 absorption led to an increased reduction of ionic substances at the cathode, causing the anode to dissolve and generate more Fe^{2+5}. In contrast, in DETA solutions, as the CO_2 loading rose from 0.4 to 1.2 mol/mol, the corrosion rates of 20# carbon steel gradually decreased. This phenomenon was associated with the potent ability of DETA to complex with Fe^{2+}. At low CO_2 loading, more DETA molecules in the solution donated electrons to the vacant d-orbitals of iron, promoting the anode dissolution process. A comprehensive analysis is provided in Part 4.

3.2. Electrochemical Corrosion Behavior. Major metal corrosion occurs through electrochemical reactions at the metal−solution interface. Electrochemical measurements, providing information on the metal/electrolyte interface, are an effective technique for studying corrosion behavior and

https://doi.org/10.1021/acsomega.3c09540
ACS Omega 2024, 9, 13067−13080

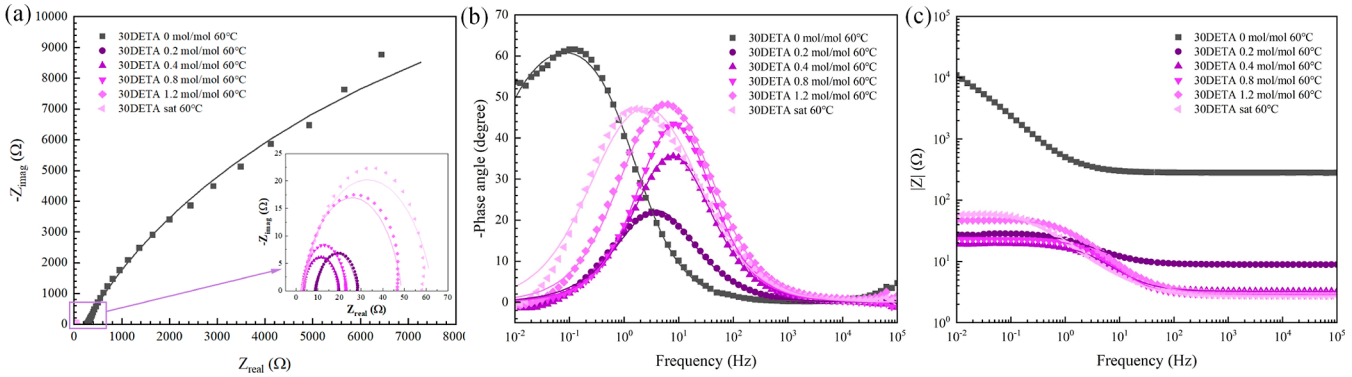

Figure 6. EIS results of 20# carbon steel in 30% DETA solutions under different conditions: (a) Nyquist plots; (b) Bode plots of impedance versus frequency; (c) Bode plots of phase angle versus frequency.

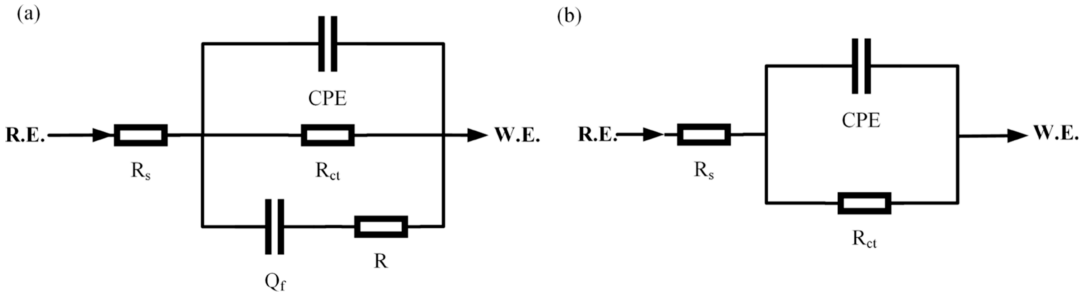

Figure 7. Electrochemical equivalent circuit (EEC) of EIS impedance spectrum in the MEA and DETA solutions: (a) fresh solutions and (b) CO_2-loaded solutions.

mechanisms.[33] The initial step in electrochemical corrosion testing is the measurement of the OCP. Adequate time is allowed for the OCP to stabilize. A stable OCP indicates that the system is in a steady state, signifying a constant speed of various corrosion reactions.

3.2.1. Tafel Curve. The Tafel curve, depicting the reaction rate of the cathode and anode, serves as a rapid and accurate method for measuring corrosion behavior at a given time. In this study, an electrochemical test was conducted for 24 h from the start. The Tafel curves of 20# carbon steel recorded in MEA and DETA solutions under different conditions are illustrated in Figures 4a and 5a. The fitted electrochemical parameters [corrosion potential (E_{corr}), corrosion current (i_{corr}), cathode (β_c) and anode (β_a) Tafel slopes, CR, etc.] are listed in Table 3.

Figure 4a illustrates that in fresh MEA solutions, the corrosion current was negligible, signifying almost no corrosiveness to carbon steel. This aligns with the weight loss method results. However, when the CO_2 loading reached 0.4 mol/mol, the Tafel curve changed significantly. According to the Tafel slopes of the cathode and anode obtained by extrapolation listed in Table 3, the slopes of the cathode curves under the three MEA concentrations were greater than those of the anode, which indicated that the corrosion process was mainly controlled by the cathode reaction. In addition, as the amine concentration increased, the Tafel slope of the cathode increased, and the corrosion current increased, resulting in a higher CR. This is attributed to the fact that more reducing species were contained in the solution with higher amine concentration, accelerating the cathodic reaction and subsequently increasing the corrosion current.

In DETA solutions, the corrosion process exhibited greater complexity. Tafel curves for 30% DETA solutions, after 24 h of corrosion under various CO_2 loadings and temperatures, were analyzed. Similar to MEA solutions, fresh DETA solutions showed minimal corrosion currents, indicating low corrosiveness. Yet, as the CO_2 loading increased from 0.4 to 1.2 mol/mol, the corrosion current exhibited a declining trend, correlating with a reduced CR. The Tafel curve indicated that the corrosion potential became more negative at 0.4 mol/mol, signifying increased metal dissolution and heightened corrosion activity.[19] Both cathode and anode polarization curves shifted upward, indicating intensified reactions at both interfaces. Comparing the Tafel slope of 20# carbon steel in DETA solutions with different CO_2 loadings, it is found that it continued to increase with decreasing CO_2 loading, indicating a faster kinetic process. Under low loading conditions, the larger Tafel slope explained the higher corrosion current and CR, allowing the anode to dissolve quickly.[31] This was related to the strong complexing ability of DETA with metal ions and corresponded to the weight loss results. Temperature effects are evident in Figure 5, where higher temperatures accelerated both anodic and cathodic polarization curves, expediting the reaction rate in MEA solutions.

3.2.2. Electrochemical Impedance Spectroscopy. To delve deeper into the corrosion behavior of 20# carbon steel in CO_2-loaded amine solutions and the electrochemical behavior of the metal/solution interface, EIS measurements were conducted.

Figure 4 displays Nyquist and Bode plots illustrating the corrosion of 20# carbon steel in MEA solutions. Fresh solutions exhibited three incomplete semicircles in Nyquist plots (Figure 4b), indicating constant |Z| values in the low-frequency range (Figure 4c). The Bode plots (Figure 4d) showed phase angles decreasing to 0° at high frequencies due to the electrolyte resistance response, with a small peak at low frequencies. For MEA solutions with CO_2 loadings, Nyquist plots displayed a single capacitive loop, signifying a charge-transfer process

https://doi.org/10.1021/acsomega.3c09540
ACS Omega 2024, 9, 13067−13080

Table 4. Fitted EIS Parameters of Electrical Equivalent Circuit for 20# Carbon Steel in Different Solutions

condition				CPE ($F \cdot cm^{-2}$)				
medium	temperature (°C)	CO_2 loading (mol/mol)	R_s ($\Omega \cdot cm2$)	$Y_0 \times 10^{-5}$	n	R_{ct} ($\Omega \cdot cm^2$)	$Q_f \times 10^{-5}$ ($F \cdot cm^{-2}$)	R ($\Omega \cdot cm^2$)
30% MEA	60	0	646.3	3.45	0.887	4.07×10^5	78.7	2176
		0.4	14.48	26.8	0.780	887.8		
40% MEA		0	825.3	3.42	0.896	6.07×10^5	48.2	2906
		0.4	17.15	36.5	0.757	638.9		
50% MEA		0	1542	3.43	0.883	5.43×10^5	40.9	6181
		0.4	21.3	55.5	0.761	484.0		
30% DETA	40	1.2	51.7	24.4	0.881	557.2		
	60	0	3367	4.03	0.720	4.06×10^5	1.41	81.9
		0.4	38.98	50.3	0.833	195.7		
		0.8	33.94	36.5	0.875	243.2		
		1.2	36.04	38.7	0.814	547.7		
	80	1.2	21.32	110	0.777	128.2		

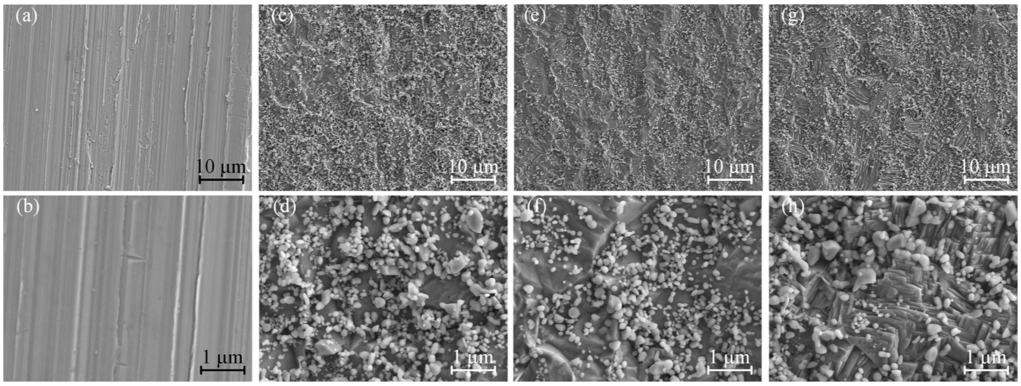

Figure 8. SEM images of carbon steel surface after 30 day corrosion treatment in 30% DETA solutions under different CO_2 loadings (60 °C): (a, b) 0 mol/mol; (c, d) 0.4 mol/mol; (e, f) 0.8 mol/mol; and (g, and h) 1.2 mol/mol.

control. The semicircle diameter decreased with rising MEA concentration, revealing reduced charge-transfer resistance and an increased CR. Bode plots showed decreased absolute impedance and phase angle relative to fresh solutions, indicating more active sites available for charge transfer.

Figure 6 presents EIS results for 20# carbon steel in DETA solutions. Fresh solutions (Figure 6a) displayed larger semicircle diameters, representing high impedance and almost noncorrosiveness. Upon CO_2 absorption, Nyquist plots exhibited semicircles with the corrosion process still predominantly controlled by charge transfer. Increasing the CO_2 loading from 0.4 to 1.2 mol/mol resulted in an increased semicircle diameter, higher charge-transfer resistance, and reduced CR, consistent with weight loss method results. The influence of temperature on EIS data confirmed that higher temperatures enhanced the corrosion reaction.

The EEC and EIS data, fitted using Gamry Analysis software, are presented in Figure 7 and Table 4. In the EEC of fresh solutions (Figure 7a), R_s denotes the solution resistance, constant phase element (CPE) represents a CPE associated with the double-layer capacitance, and R_{ct} signifies the charge-transfer resistance. R stands for polarization resistance, and Q_f refers to the double-layer capacitance at the interface between 20# carbon steel and the solutions within the film pores. Notably, the R_s values in fresh amine solutions were substantial, suggesting low conductivities. The R_{ct} values exhibited a high order of magnitude, implying that the lower the CR of 20# carbon steel, the more significant the hindrance of charge-transfer resistance.[34] Integrating weight loss method, Tafel curve, and EIS results validated the noncorrosive nature of fresh amine solutions to the equipment.

The EEC for corrosion in CO_2-loaded amine solutions is depicted in Figure 7b. As no protective film was observed on specimen surfaces in corrosion experiments with the two amine solutions, R_s represents the solution resistance in the EEC, graphically determined from the real (X) axis intercept at a high frequency in the Nyquist plots. Lower R_s values indicated a high conductivity in all solutions. The charge-transfer resistance R_{ct} could be directly determined from the semicircle diameter of the Nyquist plots. To optimize the fit, a CPE was used instead of double-layer capacitance (C_{dl}) to accommodate deviations from ideal capacitive behavior due to surface roughness, heterogeneity, and adsorption effects.[35] In DETA solutions, the change in R_{ct} differed from that in MEA solutions. R_{ct} increased with rising CO_2 loading, while the CPE continuously decreased. DETA, being a corrosion inhibitor due to its strong ability to bind metal ions, explained the opposite trend in corrosion rates between DETA and MEA solutions. Figure 5c,d illustrates Bode plots of 20# carbon steel in DETA solutions with varying CO_2 loadings. Across a broad frequency range from 0.01 Hz to 100 kHz, only one time constant was observed, suggesting a similar corrosion mechanism in all solutions.[36] Absolute impedance at low frequencies in Bode modulus plots increased with higher CO_2 loading in DETA solutions and decreasing temperatures, indicating improved protection of 20# carbon steel against corrosion.

3.3. Surface Characterization. The surfaces of 20# carbon steel specimens corroded in 30% MEA and 30% DETA solutions

https://doi.org/10.1021/acsomega.3c09540
ACS Omega 2024, 9, 13067−13080

(Figure 8) with different CO_2 loadings were analyzed using SEM, EDS, and XRD. No apparent protective layer of corrosion products was observed for #20 carbon steel in the MEA solution. In the EDS results, only Fe, C, and other elements from the original carbon steel were detected on specimen surfaces, with no O detected. XRD patterns showed only iron peaks on the surface of specimens (Figure 9). These results align well with the observed change in the CR of 20# carbon steel in MEA solution.

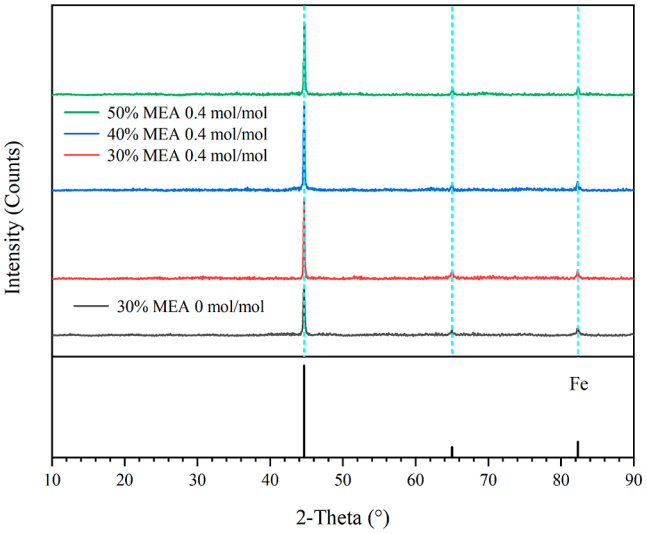

Figure 9. XRD images of 20# carbon steel surface after corrosion treatment in MEA solutions for 30 days under different conditions.

In the DETA solution, the corrosion behavior intensified. The microstructure of 20# carbon steel consisted of two phases: pearlite and ferrite. The SEM image of the specimen surface (Figure 8) reveals pearlite (Fe + Fe_3C) areas in parts c, e, and g. Given that the corrosion potential of Fe_3C is more positive than that of ferrite, a galvanic effect formed between them, leading to selective dissolution of the ferrite phase. Consequently, a significant amount of pearlite residual iron carbide (Fe_3C) remained on the carbon steel surface. As ferrite continued to dissolve, more Fe_3C was exposed, resulting in increased corrosion attacks.[35,37,38] XRD results for the surface in Figure 10 indicate that with an increase in CO_2 loading, the relative intensity of peaks for Fe_3C residues continuously decreased. A smaller amount of carbide on the surface corresponded to a lower CR,[23] consistent with weight loss method results. EDS results (Table 5) for the surface after DETA experiments with three CO_2 loadings revealed trace oxygen elements. These findings suggest that in the DETA corrosion experiment, the corrosion behavior of 20# carbon steel was more severe than that in MEA. The surface was predominantly covered by Fe_3C residues with a potential formation of a small oxide layer, even though not uniformly spread.

3.4. Precipitate Analysis. In addition to characterizing the corroded 20# carbon steel surface, precipitates were observed in some solutions during experiments. MEA solutions loaded with CO_2 became turbid, exhibiting more precipitates under all amine concentrations and temperature conditions. After suction filtration and drying into a powder, characterization tests were conducted. SEM micrographs of precipitates in MEA solutions (Figure 11) displayed variations in surface morphology at different exposure positions. The precipitates were identified as small crystalline globules or flowery plates (γ-FeOOH-

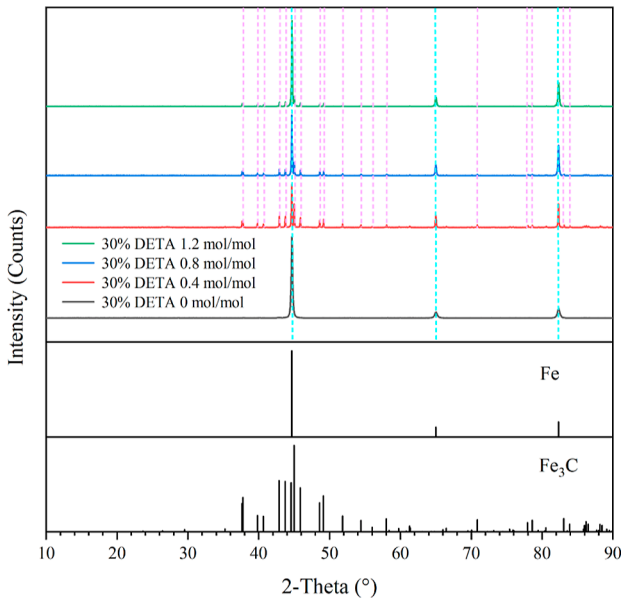

Figure 10. XRD images of 20# carbon steel surface after corrosion treatment for 30 days in 30% DETA solutions under different CO_2 loadings.

Table 5. Three EDS Analysis of 20# Carbon Steel after Corrosion in DETA Solution

	element		
conditions (mol/mol)	Fe (wt %)	C (wt %)	O (wt %)
30% DETA 0	92.29	7.33	0
30% DETA 0.4	88.60	10.04	1.04
30% DETA 0.8	89.49	9.01	1.10
30% DETA 1.2	90.21	8.22	1.25

lepidocrocite) (Figure 11a), semicrystalline spherical structures (goethite) (Figure 11b), and cotton ball-like structures (akaganeite) (Figure 11c). These SEM findings suggested that the precipitated product of 20# carbon steel in MEA solutions primarily consisted of FeO(OH) in various crystal phases, typical for carbon steel corrosion in MEA solutions under oxygen-containing conditions.[38] The XRD pattern in Figure 12 corresponds to this observation, although the baseline was not flat, possibly due to the presence of other components like Fe_2O_3, Fe_3O_4, and other oxides in small amounts that could not be clearly identified.

In the corrosion process of 20# carbon steel in DETA solutions, a minor amount of precipitates emerged, and the solutions remained clear. The collected precipitate underwent characterization. XRD results in Figure 13, coupled with literature information,[39] indicate that the predominant products were magnetite Fe_2O_3 and Fe_3O_4. The sphere cluster structure depicted in Figure 14 represented a typical morphology of γ-Fe_2O_3.[40] In the presence of oxygen, fine particles of magnetite Fe_3O_4 and less-stable γ-Fe_2O_3 could potentially transform into hematite (α-Fe_2O_3) to exist in a stable state. Hematite is a primary component of rust resulting from the corrosion of carbon steel.[39]

4. DISCUSSION

4.1. Mechanism of Corrosion. In general, amines are not inherently corrosive due to their high pH and low conductivity. However, their corrosive potential increases when they absorb

https://doi.org/10.1021/acsomega.3c09540
ACS Omega 2024, 9, 13067−13080

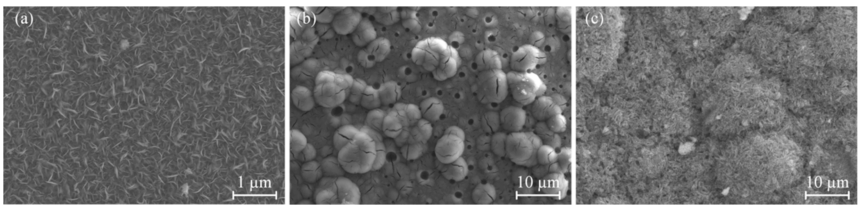

Figure 11. SEM image of precipitates after corrosion for 30 days in CO_2-loaded MEA solutions: (a) crystal ball or flowery flake (γ-FeOOH lepidocrocite); (b) semicrystalline (goethite); and (c) cotton ball (akaganeite).

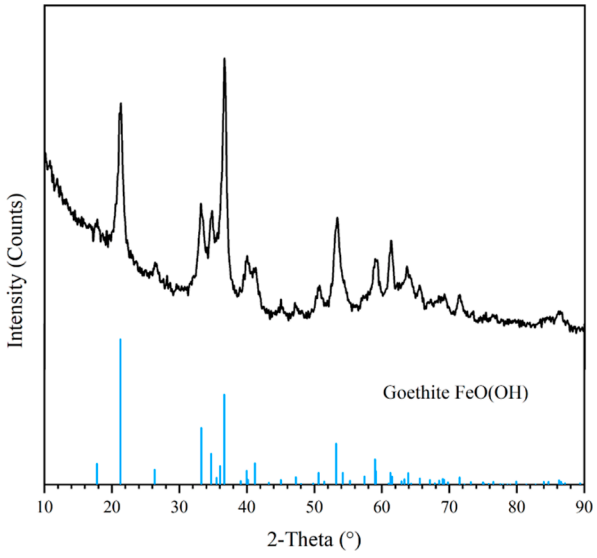

Figure 12. XRD analysis of precipitations in CO_2-loaded MEA solutions after corrosion for 30 days.

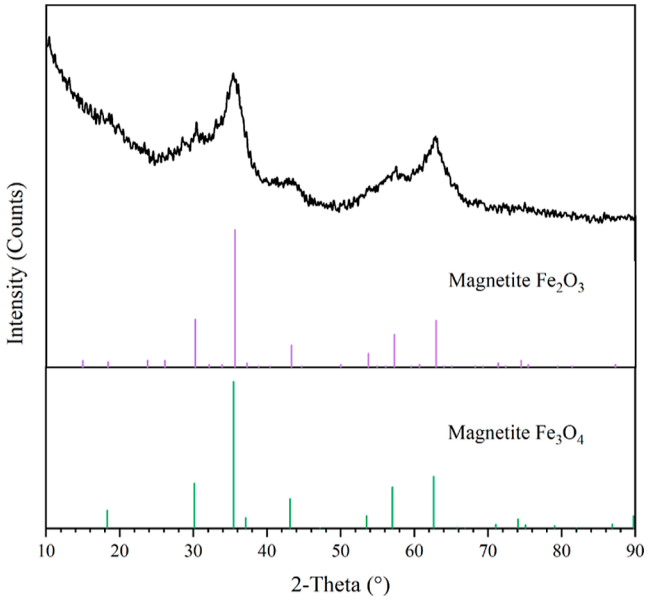

Figure 13. XRD analysis of precipitations in DETA solutions after corrosion for 30 days.

acidic gases such as CO_2. The presence of various ions in the solution can act as oxidants or reducing agents in the corrosion reaction, significantly influencing the speed and direction of the corrosion process. Numerous studies have detailed the reaction processes of amine solutions absorbing CO_2 [(R1)−(R6)].[22,41]

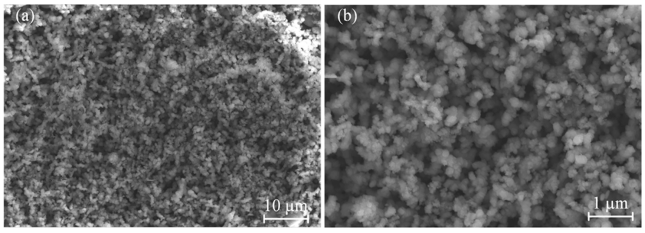

Figure 14. SEM image of precipitations in CO_2-loaded DETA solutions after corrosion for 30 days: (a) scale bar is 10 μm and (b) scale bar is 1 μm.

The CO_2 absorption process primarily involves the reaction of MEA and DETA (primarily primary amino acids) with CO_2:

Dissociation of water

$$H_2O \leftrightarrow OH^- + H^+ \quad \text{(R1)}$$

Formation of bicarbonate ions

$$CO_2 + H_2O \leftrightarrow HCO_3^- \quad \text{(R2)}$$

$$CO_2 + OH^- \leftrightarrow HCO_3^- \quad \text{(R3)}$$

Formation of carbonate ions

$$HCO_3^- \leftrightarrow H^+ + CO_3^{2-} \quad \text{(R4)}$$

Formation of the carbamate ion

$$2RR'NH_2 + CO_2 \leftrightarrow RR'NHCOO^- + RR'NH_3^+ \quad \text{(R5)}$$

Hydrolysis of the carbamate ion

$$RR'NHCOO^- + H_2O \leftrightarrow RR'NH_2 + HCO_3^- \quad \text{(R6)}$$

In the Amine-CO_2−H_2O system, the ions resulting from the reactions described previously create conditions conducive to corrosion. Typically, the corrosion process encompasses the oxidation reaction (R7) of the anode iron and the reduction reactions [(R8)−(R10)] of the cathodic species.[42]

Dissolution of anode iron

$$Fe \leftrightarrow Fe^{2+} + 2e^- \quad \text{(R7)}$$

Cathodic reaction

$$2HCO_3^- + 2e^- \leftrightarrow H_2 + 2CO_3^{2-} \quad \text{(R8)}$$

$$2H^+ + 2e^- \leftrightarrow H_2 \quad \text{(R9)}$$

$$2H_2O + 2e^- \leftrightarrow H_2 + 2OH^- \quad \text{(R10)}$$

The anions in the solution included OH^- and CO_3^{2-}, and the formation of the corrosion products was as follows

$$Fe^{2+} + CO_3^{2-} \leftrightarrow FeCO_3 \quad \text{(R11)}$$

$$Fe^{2+} + 2OH^- \leftrightarrow Fe(OH)_2 \quad \text{(R12)}$$

https://doi.org/10.1021/acsomega.3c09540
ACS Omega 2024, 9, 13067−13080

In the presence of oxygen, the cathode also underwent an O_2 reduction (R13).

Reduction of O_2

$$O_2 + 2H_2O + 4e^- \leftrightarrow 4OH^- \quad \text{(R13)}$$

Dissolved oxygen plays a significant role in influencing the corrosion of the system. It directly participates in the reduction process, contributing to an increase in the corrosion current and accelerating the dissolution of 20# carbon steel, despite its low concentration and nonprimary role in the reduction reactions. Furthermore, the presence of dissolved oxygen hinders the formation of a protective layer, potentially a key factor in the pronounced corrosion observed in CO_2-loaded amine solutions.[43] In the presence of dissolved oxygen, Fe^{2+} becomes unstable, with some undergoing further oxidation to Fe^{3+} (R14). Subsequently, Fe^{3+} can give rise to insoluble corrosion products, such as $Fe(OH)_3$, in contrast to other possible precipitates like $FeCO_3$ and $Fe(OH)_2$ (R15). The precipitation of $Fe(OH)_3$ and its subsequent reactions contribute to the formation of additional corrosion products.[39]

$$Fe^{2+} \leftrightarrow Fe^{3+} + e^- \quad \text{(R14)}$$

$$Fe^{3+} + 3OH^- \leftrightarrow Fe(OH)_3 \quad \text{(R15)}$$

Corrosion can be mitigated through the formation of a protective layer, such as siderite ($FeCO_3$) or magnetite (Fe_3O_4), on the surface of the carbon steel. However, the development of these protective layers is contingent upon operating conditions, including amine type, temperature, the presence of oxygen, and solution pH. The formation of $FeCO_3$ relies on the supersaturation (δ_{SD}) of Fe^{2+} and CO_3^{2-}, as outlined in eqs 3 and 4.[44] A protective layer in the form of $FeCO_3$ can precipitate or form only when the concentrations of free Fe^{2+} and/or CO_3^{2-} reach the minimum saturation (δ_{SD}) required for $FeCO_3$ formation.

$$K_{sp} = C_{Fe^{2+}}C_{CO_3^{2-}} \quad (3)$$

$$\delta_{SD} = \frac{C_{Fe^{2+}}C_{CO_3^{2-}}}{K_{sp}} \quad (4)$$

Where K_{sp} is the solubility constant of $FeCO_3$, and C_{Fe}^{2+} and C_{CO3}^{2-}, respectively, are the concentrations of free Fe^{2+} and CO_3^{2-}.

Previous studies have identified free H_2O, H^+, and HCO_3^- as the primary oxidants involved in the corrosion of MEA-CO_2 solutions.[43] In this system, the hydrolysis reaction (R6) of carbamate ions can only occur under conditions of high CO_2 absorption.[45] Localized regions near the carbon steel surface may not achieve the minimum $FeCO_3$ formation saturation degree (δ_{SD}) due to favorable carbamate formation and a low equilibrium constant between carbamate and bicarbonate, resulting in low concentrations of free Fe^{2+} and CO_3^{2-}. Characterization results further revealed that the corrosion products of CO_2-loaded MEA solutions primarily existed as precipitates with no protective film on the surface, leading to elevated corrosion rates. Fe^{2+} may undergo oxidation by dissolved oxygen in the solution to form the principal final product, Fe_2O_3, as illustrated in (R16−R18). $Fe(OH)_2$ serves as an intermediate oxidation product in this system. In the presence of oxygen, the more-stable $Fe(OH)_3$ is formed, accompanied by the production of other corrosion products such as $FeO(OH)$ and Fe_2O_3 (R19−20). Among these, $FeO(OH)$ was identified as the primary component of the precipitates after corrosion of the CO_2-loaded MEA solutions, as confirmed by SEM and XRD results.

$$2Fe^{2+} + 3H_2O \leftrightarrow Fe_2O_3 + 6H^+ + 2e^- \quad \text{(R16)}$$

$$3Fe^{2+} + 4H_2O \leftrightarrow Fe_3O_4 + 8H^+ + 8e^- \quad \text{(R17)}$$

$$2Fe_3O_4 + H_2O \leftrightarrow 3Fe_2O_3 + 6H^+ + 2e^- \quad \text{(R18)}$$

$$Fe(OH)_3 \leftrightarrow FeO(OH) + H_2O \quad \text{(R19)}$$

$$2FeO(OH) \leftrightarrow Fe_2O_3 + H_2O \quad \text{(R20)}$$

The CO_2 absorption mechanism in the DETA solution closely resembles that in the MEA solution. DETA reacts with CO_2 to form carbamates. The two primary and secondary amino groups contained in DETA make it have a stronger CO_2 absorption capacity than MEA. Hartono et al.[46] conducted ^{13}C NMR studies on DETA solutions with varying CO_2 loadings at 298.0 K. The results indicated that peaks corresponding to bicarbonate and carbonate (HCO_3^-/CO_3^{2-}) appeared only at a loading of 1.39. In systems with CO_2 loadings less than 1.0, carbamates were the predominant species formed, with no HCO_3^-/CO_3^{2-} observed. Hence, under the investigated CO_2 loading conditions, DETA carbamates hardly underwent hydration. Furthermore, Figure 16 illustrates that the concentration of Fe^{2+} in the DETA solution was significantly higher than that in the MEA solution, suggesting that most of the Fe^{2+} was dissolved in the solution, explaining the lack of precipitation. DETA, being a long-chain aliphatic amine, possesses inherent corrosion-inhibitory effects, and its strong complexing ability with metal ions may result in a higher solubility of Fe^{2+} in DETA solutions. Consequently, free Fe^{2+} and CO_3^{2-} concentrations do not accumulate sufficiently to form the $FeCO_3$ protective layer (δ_{SD}). The small amounts of precipitation observed in the SEM and XRD results can also be explained by the corrosion mechanism of carbon steel in MEA solutions. Additionally, the hydroxide in (R15) undergoes several phase transitions, with the final stable product existing in the phase structure of α-Fe_2O_3.

4.2. Effects of CO_2 Loading on CR of 20# Carbon Steel in DETA Solutions. An intriguing observation from the results is the decrease in the CR of 20# carbon steel in DETA solutions with increasing CO_2 loadings. This section delves into a detailed analysis of this phenomenon.

4.2.1. With or without CO_2 Loading. The three amino groups in DETA endow it with a robust CO_2 absorption capacity. Ionic species generated during this process act as oxidants in the corrosion reaction, promoting anode oxidation. Therefore, once the absorption of CO_2 occurs, a tendency for corrosion emerges. Notably, fresh DETA solutions without CO_2 loading did not corrode the 20# carbon steel specimens.

4.2.2. Complexation of DETA Molecules and Metal Ions. The strong complexation of DETA with metal ions may be the main reason for the different phenomena between the DETA and MEA solutions. The chemisorption of amine derivative molecules on the carbon steel #20 surface is driven by donor−acceptor interactions between the lone pair electrons of nitrogen atoms and the vacant d-orbitals of iron (Figure 15).[47] The process is influenced by physicochemical properties such as functional groups, electron density at the donor atoms, and electronic structure of the molecule.[48]

Saha et al.[49] employed Frontier molecular orbital theory to calculate the interaction between three organic amine corrosion inhibitors and metal atoms. The study highlighted the role of the

https://doi.org/10.1021/acsomega.3c09540
ACS Omega 2024, 9, 13067−13080

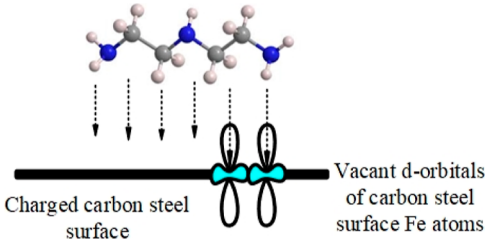

Figure 15. Interaction between DETA and the carbon steel surface through chemical adsorption processes.

highest occupied molecular orbital (HOMO) and lowest unoccupied molecular orbitals (LUMOs) in explaining the reactivity of the inhibitor molecules. Higher HOMO values indicate better electron-donating ability, while lower LUMO values facilitate stronger adsorption onto metal surfaces. The energy gap ($\Delta E = E_{LUMO} - E_{HOMO}$) serves as a fundamental quantum chemical parameter, with lower ΔE values correlating with higher reactivity and enhanced adsorption on metal surfaces, ultimately leading to higher corrosion inhibition efficiency. The results showed that the E_{HOMO} value increased with the increasing length of the amine molecular chain and the number of nitrogen atoms, indicating their electron donation ability in the order of PEHA > TETA > DETA. The E_{LUMO} value comparison order was DETA > TETA > PEHA, which meant an increase in electron acceptance ability. In addition, results from MD simulations indicated that DETA molecules possess a strong electron-donating ability. Adsorption of DETA molecules onto a metal surface through relaxed adsorption released a significant interaction energy of −355.30 kJ/mol, emphasizing the molecule's strong surface adsorption capacity. The high interaction energy suggests that DETA molecules are prone to spontaneous adsorption onto metal surfaces.

In the CO_2 capture process, relatively high amine concentrations are required, such as 2.5 M (~25.56 wt %), as used in the trail pilot plant[50] and this work. The DETA contents in solutions with different CO_2 loadings used in this experiment were calculated based on the theoretical maximum CO_2 absorption capacity of DETA, as shown in Table 6. It can be

Table 6. DETA Molecule Concentration in Solutions with Different CO_2 Loadings

condition	CO_2 loading (mol/mol)	DETA concentration (ppm)
30% DETA	0	300,000
	0.4	220,000
	0.8	140,000
	1.2	60,000

understood that at low CO_2 loading (0.4 mol/mol), there were more free DETA molecules in the solution. Excess DETA facilitated complexation with iron ions, intensifying the anode dissolution reaction, as observed in the Tafel curve in Figure 5. Figure 16 illustrates the concentration of iron ions in amine solutions after corrosion experiments under various conditions, as measured by spectrophotometry. The high solubility of Fe^{2+} was a contributing factor, preventing the formation of a protective film, thereby intensifying the corrosion behavior. This finding aligns with the results obtained by Fytianos G's et al.,[51] who observed that higher iron solubility in amine solutions led to less $FeCO_3$ formation and a higher CR. Among the five tested amines, DETA exhibited the highest corrosiveness and the highest Fe^{2+} solubility.

In addition, the pH value of the test solution before and after the weight loss method experiment was measured, as shown in Figure 17. The pH of the DETA solution before the experiment showed a downward trend with the increase of CO_2 loading due to the different contents of acidic gas CO_2 absorbed. After the 30 day soaking experiment, the CO_2-loaded samples all experienced varying degrees of pH decline. This was because the metal ion is a Lewis acid, and the pH of the solution decreased the most under low CO_2 loading, indicating that there are the most iron ions in the solution under this condition, which corresponded to the results in Figure 16. In MEA solutions, the increase in the CO_2 loading reduced the solution pH, and the reducing substances in the solution increased, which increased the CR. In the DETA solution, not only did the absorption of CO_2 cause the cathode reaction to accelerate but the complexation of DETA and iron ions caused the anode to quickly dissolve. The combined effect of the two made the impact of CO_2 loading on the CR showing a different trend from that of MEA. Despite this, when the DETA solution has the same amino CO_2 loading as MEA (0.4 C/N), the CR of the DETA is much greater than that of MEA (1.146 mm/a > 0.225 mm/a).

4.2.3. Unable to Form Protective Film. Finally, the inability to form a $FeCO_3$ protective film through CO_2 absorption resulted in a relatively high CR of 20# carbon steel in DETA solutions. Most iron ions dissolved in DETA solutions, leading to insufficient concentrations of free Fe^{2+} and CO_3^{2-} to facilitate the formation of a protective film, as explained in the Mechanism of Corrosion section.

5. CONCLUSIONS

This study comprehensively assessed the corrosion behavior of 20# carbon steel in DETA solutions under varying temperatures and CO_2 loadings, comparing it with MEA solutions. The evaluation incorporated weight loss analysis, Tafel tests, and EIS, coupled with characterizations via SEM, XRD, and spectrophotometry. The exploration of the corrosion reaction mechanism yielded the following key findings.

1 From the perspective of CR, the corrosion behavior of 20# carbon steel in DETA solutions exhibited greater severity compared to MEA solutions. As the temperature increased, both the anode and cathode reaction rates accelerated, leading to a continuous rise in the CR. Contrary to MEA solutions, the trend in the CR change differed in DETA solutions with increasing CO_2 loading.

2 The electrochemical results showed that the corrosion process in DETA solutions was exclusively controlled by charge transfer, without diffusion control. Simultaneously, the increase in corrosion current was jointly influenced by cathodic and anodic reactions.

3 As in MEA solutions, the corrosion process in DETA solutions failed to form a protective film. This lack of film formation was attributed to concentrations of free Fe^{2+} and CO_3^{2-} not reaching the required minimum saturation degree for $FeCO_3$ protective film formation. The presence of O_2 exacerbated the formation of nonprotective iron oxides.

4 With DETA CO_2 loading increasing from 0.2 mol/mol to 1.2 mol/mol, the CR of 20# carbon steel decreased continuously. DETA's strong complexing ability with metal ions resulted in higher solubility of Fe^{2+} in DETA

https://doi.org/10.1021/acsomega.3c09540
ACS Omega 2024, 9, 13067−13080

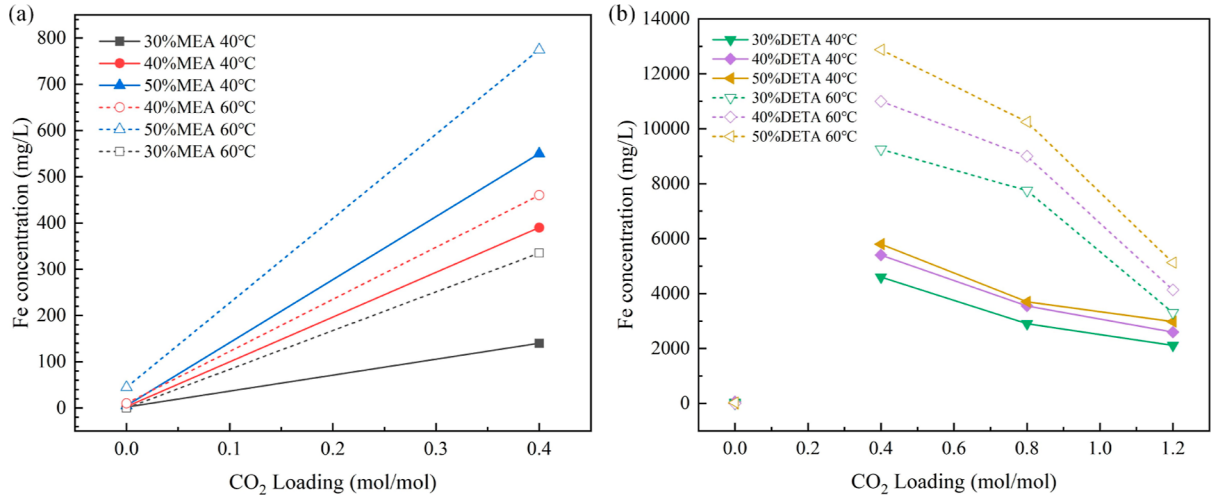

Figure 16. Concentration of iron ions in solutions after corrosion for 30 days under different conditions: (a) in MEA and (b) DETA solutions.

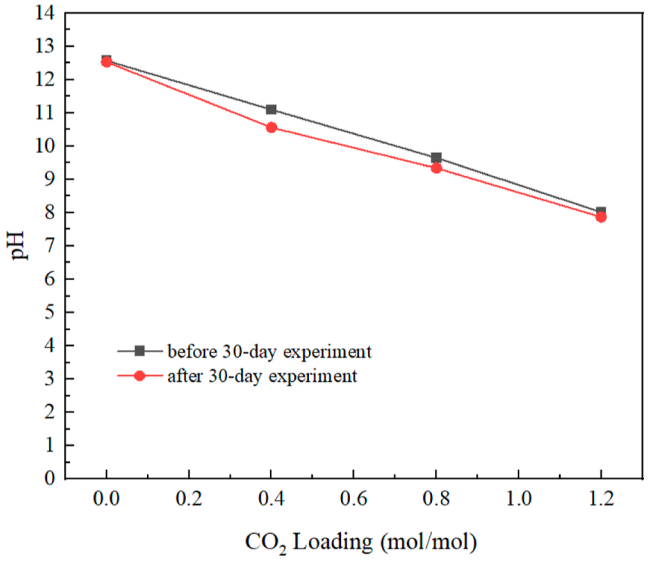

Figure 17. pH values of 30% DETA solution with different CO_2 loadings before and after a 30 day weight loss experiment at 60 °C.

solutions. Under low CO_2 loading, excess DETA promoted continuous anode dissolution, intensifying corrosion behavior.

These findings offer valuable insights into the corrosion behavior and mechanisms of carbon steel in DETA solutions, providing pertinent information for large-scale applications in carbon capture processes. Additionally, this study lays a theoretical foundation for the development of corrosion inhibitors in relevant industrial processes.

AUTHOR INFORMATION

Corresponding Author

Shujuan Wang − *Department of Energy and Power Engineering, Tsinghua University, Beijing 100084, China; Key Laboratory of Thermal Science and Power Engineering of Ministry of Education and Engineering Research Center for Ecological Restoration and Carbon Fixation of Saline-Alkaline and Desert Land, Tsinghua University, Beijing 100084, China; Shanxi Research Institute for Clean Energy, Tsinghua University, Taiyuan 030000, China;* orcid.org/0000-0001-8495-3703; Email: wangshuj@tsinghua.edu.cn

Authors

Xinyue Chen − *Department of Energy and Power Engineering, Tsinghua University, Beijing 100084, China; Key Laboratory of Thermal Science and Power Engineering of Ministry of Education, Tsinghua University, Beijing 100084, China*

Yongkang Cui − *Department of Energy and Power Engineering, Tsinghua University, Beijing 100084, China; Key Laboratory of Thermal Science and Power Engineering of Ministry of Education, Tsinghua University, Beijing 100084, China*

Complete contact information is available at: https://pubs.acs.org/10.1021/acsomega.3c09540

Notes

The authors declare no competing financial interest.

ACKNOWLEDGMENTS

This work was financially supported by National Key Research and Development Program of China (2022YFE0197800) and Common Key Projects of Shanxi Research Institute for Clean Energy Tsinghua University (2023JG0301006).

REFERENCES

(1) Mikhaylov, A.; Moiseev, N.; Aleshin, K.; Burkhardt, T. Global Climate Change and Greenhouse Effect. *JESI* **2020**, 7 (4), 2897−2913.
(2) Paltsev, S.; Morris, J.; Kheshgi, H.; Herzog, H. Hard-to-Abate Sectors: The Role of Industrial Carbon Capture and Storage (CCS) in Emission Mitigation. *Appl. Energy* **2021**, *300*, 117322.
(3) Chao, C.; Deng, Y.; Dewil, R.; Baeyens, J.; Fan, X. Post-Combustion Carbon Capture. *Renewable Sustainable Energy Rev.* **2021**, *138*, 110490.
(4) Mondal, M. K.; Balsora, H. K.; Varshney, P. Progress and Trends in CO2 Capture Separation Technologies: A Review. *Energy* **2012**, *46* (1), 431−441.
(5) Zhao, F.; Cui, C.; Dong, S.; Xu, X.; Liu, H. An Overview on the Corrosion Mechanisms and Inhibition Techniques for Amine-Based Post-Combustion Carbon Capture Process. *Sep. Purif. Technol.* **2023**, *304*, 122091.
(6) Saeed, I. M.; Alaba, P.; Mazari, S. A.; Basirun, W. J.; Lee, V. S.; Sabzoi, N. Opportunities and Challenges in the Development of Monoethanolamine and Its Blends for Post-Combustion CO2 Capture. *Int. J. Greenhouse Gas Control* **2018**, *79*, 212−233.

(7) Xiang, Y.; Choi, Y.-S.; Yang, Y.; Nešić, S. Corrosion of Carbon Steel in MDEA-Based CO $_2$ Capture Plants Under Regenerator Conditions: Effects of O $_2$ and Heat-Stable Salts. *CORROSION* **2015**, *71* (1), 30−37.
(8) An, S.; Huang, X.; Li, N.; Li, Q.; Wang, R.; Qi, T.; Wang, L. Comprehensive Performance of a Diethylenetriamine/2-Diethylaminoethanol Biphasic Absorbent for CO2 Capture. *Fuel* **2023**, *353*, 129178.
(9) Xu, M.; Wang, S.; Xu, L. Screening of Physical-Chemical Biphasic Solvents for CO2 Absorption. *Int. J. Greenhouse Gas Control* **2019**, *85*, 199−205.
(10) Xu, M.; Wang, S.; Xu, L. N $_2$ O Solubility in and Density and Viscosity of Novel Biphasic Solvents for CO $_2$ and Their Phase Separation Accelerators from 293.15 to 333.15 K. *J. Chem. Eng. Data* **2020**, *65* (2), 598−608.
(11) Zhou, X.; Li, X.; Wei, J.; Fan, Y.; Liao, L.; Wang, H. Novel Nonaqueous Liquid-Liquid Biphasic Solvent for Energy-Efficient Carbon Dioxide Capture with Low Corrosivity. *Environ. Sci. Technol.* **2020**, *54* (24), 16138−16146.
(12) Migahed, M. A.; Attia, A. A.; Habib, R. E. Study on the Efficiency of Some Amine Derivatives as Corrosion and Scale Inhibitors in Cooling Water Systems. *RSC Adv.* **2015**, *5* (71), 57254−57262.
(13) Liu, D.; Qiu, Y. B.; Tomoe, Y.; Bando, K.; Guo, X. P. Interaction of Inhibitors with Corrosion Scale Formed on N80 Steel in CO $_2$ -saturated NaCl Solution. *Mater. Corros.* **2011**, *62* (12), 1153−1158.
(14) Mahmmod, A. A.; Khadom, A. A.; Mahood, H. B. Experimental Modeling of Inhibition's Mechanism of Cupronickel Alloy by DETA and EDA into Acid Corrosive Media. *J. Bio Tribo Corros* **2020**, *6* (3), 85.
(15) Khadom, A. A. Quantum Chemical Calculations of Some Amines Corrosion Inhibitors/ Copper Alloy Interaction in Hydrochloric Acid. *J. Mater. Environ. Sci.* **2017**, *8* (4), 1153−1160.
(16) Fytianos, G.; Ucar, S.; Grimstvedt, A.; Hyldbakk, A.; Svendsen, H. F.; Knuutila, H. K. Corrosion and Degradation in MEA Based Post-Combustion CO2 Capture. *Int. J. Greenhouse Gas Control* **2016**, *46*, 48−56.
(17) Zheng, L.; Landon, J.; Zou, W.; Liu, K. Corrosion Benefits of Piperazine As an Alternative CO $_2$ Capture Solvent. *Ind. Eng. Chem. Res.* **2014**, *53* (29), 11740−11746.
(18) Zheng, L.; Matin, N. S.; Landon, J.; Thomas, G. A.; Liu, K. CO2 Loading-Dependent Corrosion of Carbon Steel and Formation of Corrosion Products in Anoxic 30 Wt.% Monoethanolamine-Based Solutions. *Corros. Sci.* **2016**, *102*, 44−54.
(19) Rafat, A.; Atilhan, M.; Kahraman, R. Corrosion Behavior of Carbon Steel in CO $_2$ Saturated Amine and Imidazolium-Ammonium- and Phosphonium-Based Ionic Liquid Solutions. *Ind. Eng. Chem. Res.* **2016**, *55* (2), 446−454.
(20) Nainar, M.; Veawab, A. Corrosion in CO $_2$ Capture Process Using Blended Monoethanolamine and Piperazine. *Ind. Eng. Chem. Res.* **2009**, *48* (20), 9299−9306.
(21) Fischer, K. B.; Daga, A.; Hatchell, D.; Rochelle, G. T. MEA and Piperazine Corrosion of Carbon Steel and Stainless Steel. *Energy Procedia* **2017**, *114*, 1751−1764.
(22) Hayfron-Benjamin, E. Characterization of Corrosion Patterns of Stainless Steel in Diethylenetriamine (DETA)-CO2 and Amine Degradation Products Systems: And an Introductory Modeling Approach. Master Thesis, Institutt for kjemisk prosessteknologi, 2013, https://ntnuopen.ntnu.no/ntnu-xmlui/handle/11250/248499 (accessed May 05 2023).
(23) Xiang, Y.; Xie, W.; Ni, S.; He, X. Comparative Study of A106 Steel Corrosion in Fresh and Dirty MEA Solutions during the CO2 Capture Process: Effect of NO3-. *Corros. Sci.* **2020**, *167*, 108521.
(24) Krzemień, A.; Więckol-Ryk, A.; Smoliński, A.; Koteras, A.; Więcław-Solny, L. Assessing the Risk of Corrosion in Amine-Based CO2 Capture Process. *J. Loss Prev. Process Ind.* **2016**, *43*, 189−197.
(25) Zheng, L.; Landon, J.; Matin, N.; Li, Z.; Qi, G.; Liu, K. Corrosion Behavior of Carbon Steel in Piperazine Solutions for Post-Combustion CO $_2$ Capture. *ECS Trans.* **2014**, *61* (20), 81−95.
(26) Campbell, K. L. S.; Zhao, Y.; Hall, J. J.; Williams, D. R. The Effect of CO2-Loaded Amine Solvents on the Corrosion of a Carbon Steel Stripper. *Int. J. Greenhouse Gas Control* **2016**, *47*, 376−385.
(27) Pearson, P.; Hollenkamp, A. F.; Meuleman, E. Electrochemical Investigation of Corrosion in CO2 Capture Plants-Influence of Amines. *Electrochim. Acta* **2013**, *110*, 511−516.
(28) Xiang, Y.; Yan, M.; Choi, Y.-S.; Young, D.; Nesic, S. Time-Dependent Electrochemical Behavior of Carbon Steel in MEA-Based CO 2 Capture Process. *Int. J. Greenhouse Gas Control* **2014**, *30*, 125−132.
(29) Gao, J.; Wang, S.; Sun, C.; Zhao, B.; Chen, C. Corrosion Behavior of Carbon Steel at Typical Positions of an Amine-Based CO_2 Capture Pilot Plant. *Ind. Eng. Chem. Res.* **2012**, *51* (19), 6714−6721.
(30) Sadeek, S. A.; Bedoya-Lora, F. E.; Campbell, K. S.; Kelsall, G. H.; Hankin, A. Formation of Protective Surface Films on Carbon Steel in Mildly Alkaline Aqueous Alkanolamine CO2 Solutions. *Corros. Sci.* **2023**, *211*, 110859.
(31) Wu, K.; Zhou, X.; Wu, X.; Lv, B.; Jing, G.; Zhou, Z. Understanding the Corrosion Behavior of Carbon Steel in Amino-Functionalized Ionic Liquids for CO2 Capture Assisted by Weight Loss and Electrochemical Techniques. *Int. J. Greenhouse Gas Control* **2019**, *83*, 216−227.
(32) Yu, L. C. Y.; Sedransk Campbell, K. L.; Williams, D. R. Carbon Steel Corrosion in Piperazine-Promoted Blends under CO 2 Capture Conditions. *Int. J. Greenhouse Gas Control* **2016**, *55*, 144−152.
(33) Tang, Y.; Guo, X. P.; Zhang, G. A. Corrosion Behaviour of X65 Carbon Steel in Supercritical-CO2 Containing H2O and O2 in Carbon Capture and Storage (CCS) Technology. *Corros. Sci.* **2017**, *118*, 118−128.
(34) Hamah-Ali, B.; Ali, B. S.; Yusoff, R.; Aroua, M. K. Corrosion of Carbon Steel in Aqueous Carbonated Solution of MEA/ [Bmim] [DCA]. *Int. J. Electrochem. Sci.* **2011**, *6* (1), 181−198.
(35) Sun, J. B.; Zhang, G. A.; Liu, W.; Lu, M. X. The Formation Mechanism of Corrosion Scale and Electrochemical Characteristic of Low Alloy Steel in Carbon Dioxide-Saturated Solution. *Corros. Sci.* **2012**, *57*, 131−138.
(36) Li, X.; Pearson, P.; Yang, Q.; Puxty, G.; Feron, P.; Xiao, D. A Study of Designer Amine 4-Amino-1-Propyl-Piperidine against the Corrosion of Carbon Steel for Application in CO2 Capture. *Int. J. Greenhouse Gas Control* **2020**, *94*, 102929.
(37) Onyeji, L.; Mohammed, S.; Kale, G. Electrochemical Response of Micro-Alloyed Steel under Potentiostatic Polarization in CO2 Saturated Brine. *Corros. Sci.* **2018**, *138*, 146−153.
(38) De La Fuente, D.; Díaz, I.; Simancas, J.; Chico, B.; Morcillo, M. Long-Term Atmospheric Corrosion of Mild Steel. *Corros. Sci.* **2011**, *53* (2), 604−617.
(39) Zheng, L.; Landon, J.; Matin, N. S.; Thomas, G. A.; Liu, K. Corrosion Mitigation via a pH Stabilization Method in Monoethanolamine-Based Solutions for Post-Combustion CO2 Capture. *Corros. Sci.* **2016**, *106*, 281−292.
(40) Ghasemi, E.; Sillanpää, M. Ultrasound-Assisted Solid-Phase Extraction of Parabens from Environmental and Biological Samples Using Magnetic Hydroxyapatite Nanoparticles as an Efficient and Regenerable Nanosorbent. *Microchim. Acta* **2019**, *186* (9), 622.
(41) Meng, F.; Meng, Y.; Ju, T.; Han, S.; Lin, L.; Jiang, J. Research Progress of Aqueous Amine Solution for CO2 Capture: A Review. *Renewable Sustainable Energy Rev.* **2022**, *168*, 112902.
(42) Soosaiprakasam, I. R.; Veawab, A. Corrosion and Polarization Behavior of Carbon Steel in MEA-Based CO2 Capture Process. *Int. J. Greenhouse Gas Control* **2008**, *2* (4), 553−562.
(43) Kladkaew, N.; Idem, R.; Tontiwachwuthikul, P.; Saiwan, C. Corrosion Behavior of Carbon Steel in the Monoethanolamine-H_2O-CO_2-O_2-SO_2 System: Products, Reaction Pathways, and Kinetics. *Ind. Eng. Chem. Res.* **2009**, *48* (23), 10169−10179.
(44) Berntsen, T.; Seiersten, M.; Hemmingsen, T. Effect of FeCO3 Supersaturation and Carbide Exposure on the CO2 Corrosion Rate of Carbon Steel. *Corrosion* **2013**, *69* (6), 601−613.
(45) Veawab, A.; Tontiwachwuthikul, P.; Chakma, A. Corrosion Behavior of Carbon Steel in the CO $_2$ Absorption Process Using

https://doi.org/10.1021/acsomega.3c09540
ACS Omega 2024, 9, 13067−13080

Aqueous Amine Solutions. *Ind. Eng. Chem. Res.* **1999**, *38* (10), 3917−3924.
(46) Hartono, A.; Da Silva, E. F.; Grasdalen, H.; Svendsen, H. F. Qualitative Determination of Species in DETA-H_2O-CO_2 System Using ^{13}C NMR Spectra. *Ind. Eng. Chem. Res.* **2007**, *46* (1), 249−254.
(47) Tan, F.; Li, K.; Yu, H.; Jiang, K.; Han, Y.; Wang, X.; Zhai, R.; Li, Y.; Chen, J. Metal ions mediated amine-based post-combustion CO2 capture. *CIESC J.* **2021**, *72* (2), 1026−1035.
(48) Veawab, A.; Tontiwachwuthikul, P.; Chakma, A. Investigation of Low-Toxic Organic Corrosion Inhibitors for CO_2 Separation Process Using Aqueous MEA Solvent. *Ind. Eng. Chem. Res.* **2001**, *40* (22), 4771−4777.
(49) Saha, S. Kr.; Murmu, M.; Murmu, N. C.; Obot, I. B.; Banerjee, P. Molecular Level Insights for the Corrosion Inhibition Effectiveness of Three Amine Derivatives on the Carbon Steel Surface in the Adverse Medium: A Combined Density Functional Theory and Molecular Dynamics Simulation Study. *Surf. Interfaces* **2018**, *10*, 65−73.
(50) Fytianos, G. *DETA Pilot Plant Campaign*; NTNU: Trondheim, 2013.
(51) Fytianos, G.; Ucar, S.; Grimstvedt, A.; Svendsen, H. F.; Knuutila, H. Corrosion Evaluation of MEA Solutions by SEM-EDS, ICP-MS and XRD. *Energy Procedia* **2016**, *86*, 197−204.

https://doi.org/10.1021/acsomega.3c09540
ACS Omega 2024, 9, 13067−13080